Nonlinear distortion of signals radiated by vibroseis sources

Andrey V. Lebedev* and Igor A. Beresnev*

ABSTRACT

A model of nonlinearity of the contact between the vibrator baseplate and the ground is proposed to describe the distortion of vibroseis signals in the near-field. A thin layer between the baseplate and the soil exhibits a strong nonlinear response because of the difference in its rigidity between the compression and tension phases. The model allows for a quantitative description of the transmission of seismic energy into the ground, including the observed harmonic distortion. However, the contact nonlinearity does not lead to the dependence of wave traveltimes on the amplitude of the force applied to the ground. This fact can be used in field observations to localize the source of the observed harmonic distortion.

INTRODUCTION

Vibroseis is the principal source of seismic energy in land exploration. To obtain high-quality earth images, it is important to achieve strict control and understanding of an outgoing signal. The problem of controlling the radiated spectrum has been considered by many authors (Lerwill, 1981; Sallas and Weber, 1982; Safar, 1984; Sallas, 1984). Most earlier works are based on the classic results of Miller and Pursey (1954), who rigorously studied the seismic radiation from a piston source at the surface of an elastic half-space. In spite of significant success in characterizing this linear problem, many practical issues arising from the field use of vibroseis sources have remained theoretically unexplained; they have typically been attributed to the nonlinearity in the complex system involving the vibrator and the ground. For example, one difficulty lies in the apparent amplitude dependence of the traveltime of radiated wavelets (Martin and Jack, 1990), while another is in the observed distortion of wavelets (Walker, 1995; Jeffryes, 1996).

Specifically, the traveltime is sometimes found to be dependent on the driving level. Martin and Jack (1990) indicate that these arrival-time variations might result from the changes in the physical properties of near-surface layers. Earlier arrival

time from a lower-energy impulse source was observed and could be considered as proof of the authors' assumption. Apparently, the soil in the near-surface layers became softer (having lower propagation velocity) as the amplitude of vibrations increased.

The second problem observed in experiments is the harmonic distortion of outgoing waves. Walker (1995) proposes to describe the distortion phenomena using a simple 1D differential equation of the Duffing type. However, such a generic model has limited practical value, since the model parameters were set arbitrarily, and the physical reason for the distortion was not clear. Also, while the differential equation could describe the vibrations of the baseplate, it did not involve the transmission of energy into the ground.

Both problems are believed to be caused by the nonlinear response of an elastic half-space or some parts of the radiating system. There are generally two viewpoints expressed in the literature regarding the range of the distances from the source at which the medium nonlinearity remains significant. One viewpoint is that there are contributions of nonlinearity to signal distortion in both the near- and far-fields of a vibrator. The harmonics are generated in the vicinity of the baseplate and continue to grow as the signal propagates as a result of the slowly accumulating nonlinear distortion of the acoustical type (e.g., Beresnev et al., 1986; Beresnev and Nikolaev, 1988; Dimitriu, 1990). However, a more common approach, for example, experimentally addressed by Jeffryes (1996), is that the near-source area is primarily responsible for the generated harmonics, while the propagation beyond this zone remains essentially linear. We follow this more commonly accepted model of soil nonlinearity in our study.

The near-source area, contributing to nonlinear distortion, could be represented as a thin layer between the baseplate and the soil where large deformations occur. This leads us to the model of contact nonlinearity, in which the effect of the layer is approximated by the response of a nonlinear oscillating spring. However, our goal is not merely to describe the oscillations of this nonlinear contact. With seismic exploration applications in mind, we are also interested in rigorously calculating the radiation of seismic energy from the contact to establish the

signature of near-source nonlinearity in seismic records. In accordance with the model, the propagation medium is assumed to be linear.

We base this approach on the substantial progress in nonlinear acoustics of solids made over the last decade (e.g., Naugolnykh and Ostrovsky, 1998; Guyer and Johnson, 1999). Nonlinearity in the generally disorganized earth materials is typically attributed to compliant features such as grain contacts, cracks, or voids, which lead to their substantial nonlinear behavior. It has been shown that the contact between oscillating solid bodies is highly nonlinear, too (Rudenko and Vu, 1994; Solodov, 1998).

The nature of contact nonlinearity could be illustrated as follows. Soil is a structurally inhomogeneous material that is in contact with the baseplate along a rough, uneven surface. The vibrations of the plate lead to the consecutive openings and closures of the contact points, so that the total contact surface is constantly changing (Solodov, 1998). This leads to the variations in an effective elastic modulus of the contact. Furthermore, the contact region is typically much softer than the other parts of the interacting bodies (the baseplate and the consolidated material below); as a result, the deformations in this intermediate region are large enough to considerably change the spectrum of radiation. A model of such a contact and its effect on the radiation are discussed below.

We should point out that the nonlinear distortions of vibroseis signals arise from two independent mechanisms: the hydraulic actuator itself and the ground nonlinearity. In this paper, we describe the distortion caused by the ground nonlinearity. For hydraulic vibrators, the actuator force itself typically carries a significant nonlinear distortion well known to engineers (e.g., Merritt, 1967). Without the loss of generality, we consider the response of nonlinear ground to the sinusoidal actuator force. Taking the actuator force in the form of a desired nonsinusoidal function for a particular vibrator type will incorporate the distortion produced by the actuator.

The feedback control systems used on modern vibrators are designed to synchronize the amplitude envelope and phase of the fundamental frequency component of the ground force to the pilot signal, although the nonlinearly generated harmonics are still radiated. These harmonics reduce the accuracy of conventional data processing, which crosscorrelates the far-field geophone signal with the pilot. Since the signal at geophones is proportional to the ground force [see equation (B-6)], the crosscorrelation ideally should be performed with the realistically distorted ground force, not the pilot, for the best deconvolution results.

This is the idea behind the processing scheme of the recently proposed high-fidelity vibratory seismic (HFVS) method (Allen, 1996; Allen et al., 1998). In the HFVS method, the ground force is recorded and is used as source signature; any harmonics generated in the source or its vicinity are included in the reference signal. The HFVS method cannot be universally utilized, though, because it requires recording and transmission of the ground-force signal at every individual shotpoint, significantly increasing the cost of the surveys, and precludes vibrator grouping, as it assumes that each vibrator has its own signature. The universal use of HFVS-type methods would ideally remove the limitations on the accuracy of vibroseis imaging caused by nonlinear distortions, both at the hydraulics and at the contact with the ground.

This article is organized as follows. In the first section, we briefly introduce the model of the vibroseis source. In the second section, a contact-type nonlinearity is incorporated. In the third section, a possible generalization of the model is discussed. This generalization includes the nonlinear response of the soil beneath the baseplate extending beyond a thin contact zone.

VIBROSEIS MODEL

In 1981, Lerwill proposed an equivalent circuit for a vibroseis source [a similar model was introduced in the 1940s in the USSR by G. Gamburtsev (Chichinin, 1984)]. Based on simple considerations valid for fluids, Lerwill proposed the equations describing the far-field of the radiated P-wave. His results were corrected by Sallas and Weber (1982) and Sallas (1984) by adding a captured mass of the ground and a formula to define the force acting on the ground. The source was considered small compared to the wavelength; it could be approximated by a 1D lumped-parameter vibratory system with masses, springs, and dashpots. All equivalent parameters of the ground in the Sallas model could be determined from the rigorous elastodynamic solutions (Miller and Pursey, 1954). The scheme considered by Lerwill (1981) and Sallas (1984) is presented in Figure 1, where z_1 is the displacement of the reaction mass and z_2 is the displacement of the baseplate. The auxiliary elements used to stabilize the baseplate are not shown [see Lerwill (1981) for the detailed description].

The ground-reaction force F_g is defined in Sallas (1984) by the acceleration of the captured mass M_g, the deformation of the captured spring K_g, and the velocity of the dashpot D_g as a result of radiation (see Figure 2).

$$-F_g = M_g \ddot{z}_2 + D_g \dot{z}_2 + K_g z_2. \tag{1}$$

This force can be determined from the measured accelerations of the reaction mass (subscript r) and the baseplate (subscript b) which is assumed inflexible (Sallas and Weber, 1982; Sallas, 1984):

$$F_g = M_r \ddot{z}_1 + M_b \ddot{z}_2. \tag{2}$$

The numeric parameters of the equivalent vibroseis circuit are listed in Table 1. These parameters, corresponding to chalk, are considered by Lerwill (1981) and Safar (1984). We use them in our numerical examples to illustrate the typical distortion associated with nonlinear soil behavior.
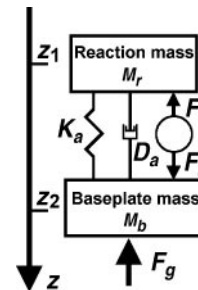

Figure 1. The scheme of the vibrator considered by Sallas (1984). The element K_a is the spring constant for the airbag suspension of the reaction mass, and D_a is the dashpot constant for the airbag, accounting for corresponding losses. The actuator force is F_a, and the ground-reaction force is F_g.

LINEAR AND NONLINEAR OSCILLATIONS OF THE VIBRATOR

Figure 2 presents a simple generalization of the Sallas model. The scheme is identical to Figure 1, except that an additional spring is added between the baseplate and the ground to describe the contact rigidity. The elements of ground reaction—K_g, M_g, and D_g—are also explicitly shown. Rudenko and Vu (1994) propose to modeling the nonlinear contact rigidity K_c by a set of small springs of variable lengths, some being out of the contact with the ground (right side of Figure 2). This model is capable of describing a wide range of nonlinear contact behavior, including the Hertz point contact (Johnson, 1985; Landau et al., 1986) and a full contact. By introducing a distribution of spring lengths (ground-roughness heights), varying degrees of contact nonlinearity can be accounted for as well.

The set of equations describing the dynamics of the system in Figure 2 is similar to that used by Sallas and Weber (1982) and Sallas (1984), with the additional restoring force F_c from the deformation of the contact spring:

$$M_r \ddot{z}_1 + D_a(\dot{z}_1 - \dot{z}_2) + K_a(z_1 - z_2) = -F_a(t),$$

$$M_b \ddot{z}_2 - D_a(\dot{z}_1 - \dot{z}_2) - K_a(z_1 - z_2) - F_c = +F_a(t),$$

$$M_g \ddot{z}_3 + D_g \dot{z}_3 + K_g z_3 + F_c = 0. \tag{3}$$

We assume the state of rest in the system as the initial condition. The term $F_a(t)$ is set to $F_a \sin \omega t$, where ω is the vibrator's operating frequency; subscripts a and b are defined in Figure 1. As stated in the Introduction, the nonlinearity in the hydraulic system is not considered in equations (3), and the actuator force is assumed sinusoidal to isolate the nonlinear distortion caused by the ground. The baseplate is assumed inflexible. The effects of the baseplate flexure on radiation will be considered in separate paper.

Equations (3) with ground force $M_g \ddot{z}_3 + D_g \dot{z}_3 + K_g z_3$ correspond to the case of small wave size of the plate (radius of the baseplate r_0 smaller than the radiated wavelengths). Otherwise, the ground reaction should be written in a more general way using the Green's function approach (Appendix C). However, we show (Figure 3) that the exact approach leads to the corrections that are negligible in the frequency range of practical interest, which justifies the use of simple equations (3).

Linear contact

We first consider the case of a linear contact with the restoring force described by Hooke's law, $F_c = K_c(z_3 - z_2)$. The ratio (transfer function) F_g/F_a as a function of frequency for this regime of vibrations is shown in Figure 3. The quantity F_g was
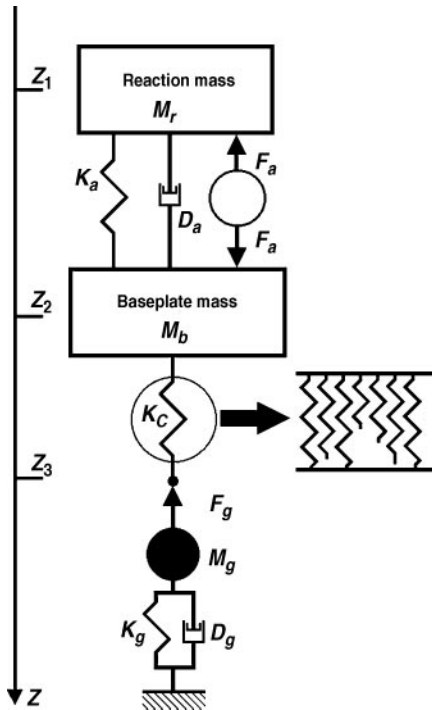

Figure 2. The circuit used as a model of nonlinear oscillations of the vibrator. The notations are as in Figure 1. The element K_c denotes the additional spring corresponding to the nonlinear contact rigidity. The horizontal arrow shows the model of the contact. The small springs have various heights; some are activated by vibrations. The quantity z_3 is the displacement of the ground.
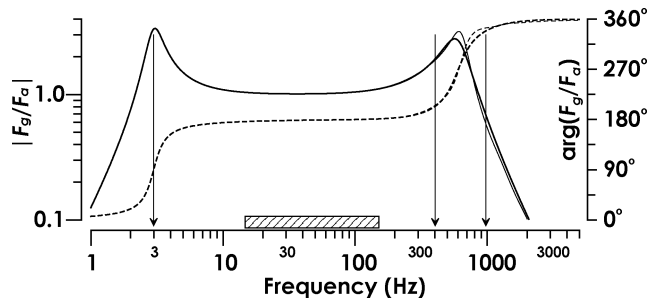

Figure 3. Ground-reaction force F_g normalized by input actuator force F_a as a function of frequency for $K_c = 10^{10}$ N/m. The other parameters are defined in Table 1. The resonance frequencies $\omega_1/2\pi = 3$ Hz, $\omega_2/2\pi = 403$ Hz, and $\omega_3/2\pi = 977$ Hz are shown by the arrows. The calculations are made for chalk. The solid and dashed lines correspond to $|F_g/F_a|$ and $\arg(F_g/F_a)$, respectively. The thin lines show the rigorous solution obtained using the Green's function method outlined in Appendix C. The horizontal bar shows the frequency interval of the sweep signal used to calculate the crosscorrelation function (see Nonlinear Contact section).

Table 1.   Parameters of the vibroseis circuit (Figure 1) used in this analysis. The value r_0 is the baseplate radius. The values of K_g, M_g, and D_g correspond to chalk with a density of $\rho = 1800$ kg/m³, an S-wave velocity of $V_S = 1235$ m/s, and a P-wave velocity of $V_P = 2140$ m/s (Šafar, 1984). The actuator force amplitude is $F_a = 79\,000$ N, corresponding to Lerwill's data (Lerwill, 1981).

r_0 (m)	K_g (N/m)	M_g (kg)	D_g (N/m/s)	K_a (N/m)	D_a (N/m/s)	M_b (kg)	M_r (kg)
0.865	1.3×10^{10}	773	7×10^6	6.25×10^5	10^4	681	1773

calculated using equation (2), with z_1, z_2 determined as the solutions of system (3). The system (3) for the linear contact was solved analytically using the standard Fourier transform technique. The resulting values of F_g were divided by F_a to obtain the thick solid line in Figure 3.

At low frequencies, the ground force [equation (2)] is dominated by the reaction-mass term $M_r \ddot{z}_1$, which becomes $M_r \ddot{z}_1 \approx \omega^2 F_a / K_a$. The ω^2 low-frequency asymptote of F_g / F_a is clearly seen in Figure 3.

One can distinguish the three resonance frequencies in the ratio, corresponding to the oscillations of the reaction mass ω_1, the oscillations of the soil near the baseplate ω_2, and the resonance of the contact ω_3. Note that the operating band of Vibroseis sources is typically between $\omega_1 / 2\pi$ and $\omega_2 / 2\pi$ (Shneerson and Mayorov, 1980; Lerwill, 1981). The frequency ω_3 was absent from the original model (Sallas and Weber, 1982; Sallas, 1984); its existence in our model reflects the inclusion of the contact spring K_c (see Figures 1 and 2). The value of K_c determines the rigidity of the contact, where it is useful to consider two limiting cases: $K_c = 0$ and $K_c = \infty$. In the first case, the contact region is very soft and the ground force is zero (the reaction mass and the baseplate vibrate without any reaction of the ground, $z_3 = 0$, $z_2 \neq 0$). Obviously, $\omega_3 \ll \omega_2$ in this case and the contact spring dominates. The second case corresponds to the full contact between the baseplate and the soil ($z_3 = z_2 \neq 0$). Here, $\omega_3 \gg \omega_2$ and the ground spring dominates. The value of $K_c = 10^{10}$ N/m corresponds to an intermediate situation of frequency ω_3 still higher than ω_2, thus modeling the situation of a well-prepared contact.

The values of the resonance frequencies were determined as the roots of the characteristic equation for system (3) after applying the Fourier transform (Landau and Lifshitz, 1976; chapters 23 and 25). This equation is a third-order polynomial with respect to ω^2:

$$-M_r M_b M_g \omega^6 + (M_r M_b (K_c + K_g) + M_r M_g (K_a + K_c)$$
$$+ M_g M_b K_a) \omega^4 - (M_r (K_a K_c + K_a K_g + K_g K_c)$$
$$+ M_b K_a (K_c + K_g) + M_g K_a K_c) \omega^2 + K_a K_c K_g = 0. \quad (4)$$

The dependence of the three resonance frequencies on ground parameters can be clarified using a simple approach. As seen from Figure 2 and for the condition $\omega_1 \ll \omega_2 \ll \omega_3$, the frequencies ω_1 and ω_2 can be thought of as the natural frequencies of the oscillations of the reaction mass attached to the actuator spring and of the combined baseplate mass and the captured mass attached to the captured spring, respectively. The frequency ω_3 similarly can be viewed as the natural frequency of the contact spring loaded with the baseplate mass on one end and the captured mass on the other end. These frequencies can then be approximated by the formulas describing oscillations of masses on a spring, $\omega_1^2 \approx K_a / M_r$, $\omega_2^2 \approx K_g / (M_b + M_g)$, and $\omega_3^2 \approx K_c (M_b + M_g) / M_b M_g$. These formulas show the parameter dependence of the resonance frequencies in a transparent manner. The values they provide, $\omega_1 / 2\pi \approx 3$ Hz, $\omega_2 / 2\pi \approx 476$ Hz, and $\omega_3 / 2\pi \approx 836$Hz, are in good agreement with the exact values obtained from equation (4) (see the exact values for the resonance frequencies in Figure 3). The heights of the peaks of the transfer function in Figure 3 will depend on the damping parameters D_a and D_g and decrease as damping increases.

The value of F_g determines the amplitudes of the emitted waves (see Appendices A and B). The result of rigorous calculations of the ground force, taking into account the finite dimensions of the source (thin line in Figure 3), is close to the results based on the approximation of ground reaction [equation (C-1)] even at high frequencies. This is an important conclusion, since the scheme of the rigorous solution of the general nonlinear problem (3) described in Appendix C is much more complicated than the solution based on equation (C-1).

In a general case of arbitrary, nonlinear spring K_c, the solution of system (3) can be obtained by numerical integration, for example, through the Runge-Kutta scheme. To check the accuracy of the scheme, we compared the numerical results with the analytical solution for the linear contact spring above. We found the relative difference between the numerical and analytical solutions of system (3) was less than 1.6×10^{-10} for the linear problem. Also, the choice of the integration step is important in numerical integration of nonlinear differential equations. Because of this, the step in all of the following calculations was varied until the solution no longer changed.

Nonlinear contact

We next consider the case of bimodular contact nonlinearity, with the restoring force in the form

$$F_c = K_1 (z_3 - z_2)$$

for

$$z_3 \leq z_2$$

and

$$F_c = K_2 (z_3 - z_2)$$

for

$$z_3 > z_2, \quad (5)$$

with $K_1 > K_2$ (stiffness in compression greater than stiffness in tension). The value of K_1 is equal to K_c for the linear contact considered above. Model (5) describes a rapid change in rigidity when compression activates the shorter spring (in the case of two different spring lengths for simplicity; see Figure 2). Note that, as stated in the Introduction, the nonlinearity is assumed to be localized at the contact, while the wave propagation from the contact is assumed to be linear.

General analysis of oscillatory systems with piecewise-linear parameters has been performed by several workers (e.g., Mahfouz and Badrakhan, 1990; Ostrovsky and Starobinets, 1995). In particular, models with bimodular elasticity are often invoked to describe strong nonlinearity in vibratory systems with backlash, a contact of one piece with another, or behavior of precompressed elements (Mahfouz and Badrakhan, 1990). The bimodular elasticity model (5) provides qualitatively similar time histories $z_j(t)$ for any amplitude of the exciting force (Mahfouz and Badrakhan, 1990; Ostrovsky and Starobinets, 1995). This means that the harmonic distortion depends on the ratio K_1 / K_2 only and not on the driving-force level. This feature is easy to understand since the constitutive law [equation (5)] only distinguishes between the compression and tension phases, in which the stiffnesses are different. Within a given phase, the stiffness is constant and does not depend on the amplitude level.

Figure 4 shows the spectral power density of the ground-reaction force and the time histories $F_g(t)$ and $F_a(t)$ for

$K_2 = 0.1K_1$. The distortion of the ground-force signal, compared to the input signal, is clear. Recall that all nonlinear distortions in Figure 4 are attributed to the contact nonlinearity, which explains the dominance of the second harmonic over the third one. In comparison, the hydraulic nonlinearity of the actuator is known to produce a stronger third harmonic.

Harmonic distortion is convenient to characterize by the parameter

$$D_{NL} = 10 \log \sum_{j=2}^{\infty} \frac{A_j}{A_1} (\text{dB}), \qquad (6)$$

where log is base 10 and A_j are the spectral power densities of harmonics. The value of D_{NL} for the ground-force signal in Figure 4 is -16 dB, which corresponds to a small contribution of harmonics to the force relative to the main tone.

The radiated power in P-, S-, and Rayleigh waves at a given frequency can be calculated from the ground force using equations (A-1), (A-2), and (A-5), respectively (Appendix A). These equations are valid for the arbitrary wave size of the baseplate. If the baseplate is small relative to the shear wavelength, the harmonic contribution will be magnified with respect to the force signal as a result of a ω^2 term in the radiated power (see Appendix A) and the distortion seen in power will increase. This is observed in Figure 4 as the magnification in the harmonic content in the total power (circles) with respect to the ground force (bars). The maximum value of magnification is 30 dB at high frequencies. This value generally depends on the operating frequency, P- and S-wave velocities in the ground, and radius of the baseplate. The magnification effect means that even small nonlinear distortion present in the force signal at the baseplate will be revealed to a much greater extent in the far-field signal. (Keep in mind, though, that the attenuation effects have not been considered in the calculation of the total radiated power.)

The time histories of the ground force and the particle velocity in the downgoing (propagating in the z-direction) P-wave are shown in Figure 5. The choice of the vertical direction is caused by the absence of S-wave contribution from potential (B-5) and the importance of downgoing radiation in practical applications. The computations were made using

equation (B-6) for each spectral component of the ground-force signal calculated earlier; consequently, the effect of anelastic attenuation is incorporated. One can observe a significant difference between the signal recorded in a borehole and F_g (Figure 5a). This difference is primarily caused by the ω-term in equation (B-6), which originates in the differentiation of the ground-force signal. Because anelastic losses for higher harmonics are greater than for the fundamental, one can expect the peaks in the far-field time history to smooth out as distance increases. If the vibroseis source operated as a linear device, the far-field and the ground-reaction force signals would be similar (Figure 5b).

So far our discussion has dealt with the solutions of equations (3) for a pure tonal input excitation. In practical applications, complex signals having wide frequency spectra, such as sweep signals, are used. As we consider a linear wave propagation problem (all nonlinearity resides in the contact spring only), we can use the superposition principle to construct the solution for complex input signals as the summation of tonal responses. We use this approach in studying the effects of contact nonlinearity on the correlation functions following; the approach is characterized as follows.

The frequencies of discrete Fourier transform are defined by

$$\omega_n = 2\pi \frac{n}{N\Delta t}, \quad n = 0, \dots, \frac{N}{2} - 1, \qquad (7)$$

where Δt is the sampling interval of $z_j(t)$ and N is the number of samples. In the following, the Fourier spectrum of the sweep signal for the ground-reaction force and far-field velocity is synthesized as a sum of the corresponding responses $z_j(t)$ in system (3) (which determine the ground force) for each frequency defined by equation (7) within the frequency band of interest. The amplitude of the acting force F_a remains the same for all frequencies. Since the signals and the crosscorrelation function are synthesized in the frequency domain, we look at the main lobe of the crosscorrelation function only; no ghosting caused by the harmonic distortion of the fundamental frequency of the sweep, appearing at regular time intervals after the main lobe (e.g., Jeffryes, 1996) is shown.
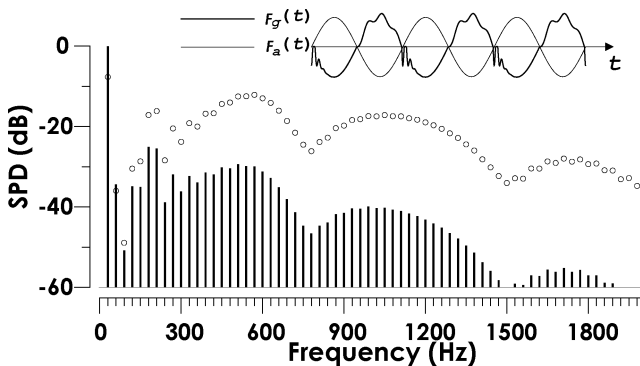

Figure 4. Fourier power spectrum of ground force for the input frequency of 30 Hz (vertical bars). The circles depict the combined power radiated in P-, S-, and Rayleigh waves. Data on both graphs are normalized by the sum of amplitudes of all harmonics. The distortion in the ground-force signal is $D_{NL} = -16$ dB. The radiated-power distortion is $D_{NL} = +8$ dB. Time histories of $F_a(t)$ and $F_g(t)$ are shown in the top right corner. SPD-spectral power density.
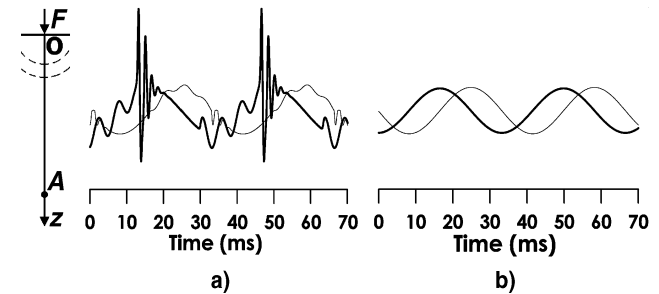

Figure 5. (a) Time histories of the particle velocity in the downgoing P-wave (thick line) and the ground-reaction force (thin line). The operating frequency of the vibrator is 30 Hz. The distance between the vibrator and the observation point $|OA| = 100$ m, which corresponds to $k_1 R \approx 10$ in equation (B-6). The anelastic losses were set to $\eta \equiv 1/Q = 0.01$, typical of consolidated soil (White, 1983). The phase shift $\exp(ik_1 R)$ in equation (B-6), which would correspond to the fundamental frequency, has been removed. (b) The same curves corresponding to the linear regime ($K_2 = K_1$) when there is no distortion. The scale of the plots is the same.

The crosscorrelation function between the far-field and the ground-force sweep signals ($C_1(\Delta t)$) is shown in Figure 6a. As stated in the Introduction, this way of processing mimics the HFVS method. The crosscorrelation between the far-field and the pilot signals ($C_2(\Delta t)$) is shown in Figure 6b, which illustrates the traditional data-processing scheme (Shneerson and Mayorov, 1980; Martin and Jack, 1990, p. 405). Since we consider only the signal distortion caused by ground nonlinearity, the pilot signal is assumed to be proportional to F_a. The crosscorrelations are calculated using the inverse fast Fourier transform. One can see that no distortion is observed in the $C_2(\Delta t)$ function (Figure 6b) because the pilot is not distorted at each emitted frequency. The function $C_2(\Delta t)$ is inverted compared with $C_1(\Delta t)$ because of the phase difference of 180° between F_g and F_a within the interval of 15 to 150 Hz, shown by the horizontal bar in Figure 3.

The width of the crosscorrelation function is inversely proportional to the frequency bandwidth of the emitted signal. A visible sharpening of $C_1(\Delta t)$ (Figure 6a) for the nonlinear oscillations is caused by the expansion of the bandwidth of both the ground-force and the far-field signals as a result of harmonics generation. However, it is clear that there is no additional delay in the arrival time because of the contact nonlinearity, in that the timing of zero crossings in both the linear and nonlinear oscillations remains unchanged (Figure 6a; the zero crossing is indicated by the vertical arrows). The absence of the delay from nonlinearity is clearly because the source of all distortion is in the force applied to the ground, not in the wave-propagation medium.

However, in the case of very strong nonlinearity (lines with circles), one can observe a delay in the traveltime for $C_2(\Delta t)$ (Figure 6b). Since this delay is absent in $C_1(\Delta t)$, it cannot be from the changes in P-wave velocity beneath the plate. Furthermore, the velocity-change effects are absent from the model considered. It is therefore important to understand the reason for this delay.

The free vibrations of a piecewise-linear oscillatory system consist of the spliced half-periods of sinusoidal functions, as illustrated in Figure 7. The top half is a sinusoidal signal with amplitude a_1 and half-period T_1 and the bottom half is a sinusoidal signal with amplitude a_2 and half-period T_2 (Ostrovsky and Starobinets, 1995). Figure 7 corresponds to the case of bimodular nonlinearity [equation (5)]. The amplitudes and periods are related through

$$\Omega_1 a_1 = \Omega_2 a_2, \qquad (8)$$

where $\Omega_{1,2} = 2\pi/T_{1,2}$ (Ostrovsky and Starobinets, 1995). The nature of the shape of the time history is clear: the system

switches from one oscillating mode to the other when the relative displacement $z_3 - z_2$ passes through zero and instantly changes the rigidity according to equation (5). The two oscillation modes thus correspond to the compression and tension phases in the system, in each of which the system oscillates in a linear manner.

The frequencies Ω_1 and Ω_2 can be determined from equation (4) with $K_c = K_{1,2}$, separately considered for the compression and tension phases. In the case of $K_2 = 0.01 K_1$, which exhibits the delay in Figure 6b, these frequencies are $\Omega_1/2\pi \equiv \omega_3/2\pi = 977$ Hz [$K_c = K_1$ in equation (4)] and $\Omega_2/2\pi = 100$ Hz [$K_c = K_2$ in equation (4)]. The latter value lies inside the frequency band of the sweep signal. Because this is the frequency of one of the system resonances, the spectral component of the sweep is amplified at this frequency and an additional phase lag also occurs (see phase of F_g/F_a in Figure 3 at resonance frequency ω_3). Because of the amplification, the effective bandwidth of the radiated signal becomes narrower, compared with the case of small difference between K_1 and K_2, and the crosscorrelation function becomes wider (Figure 6b, line with circles) in that the relative amplitudes of the side lobes become higher. The additional phase lag is revealed as a delay in the crosscorrelation function.

These values of the frequencies Ω_1 and Ω_2 do not depend on the amplitude of oscillations (the driving level) because there is only one compression rigidity and only one tension rigidity in the system, no matter how large the amplitude level (refer to the Nonlinear Contact section). So while model (5) shows the delay in the crosscorrelation function, this delay is not amplitude dependent.

The dependence of the delay on the driving level nevertheless occurs if model (5) is substituted with a more complicated nonlinear function describing the contact rigidity, in which case
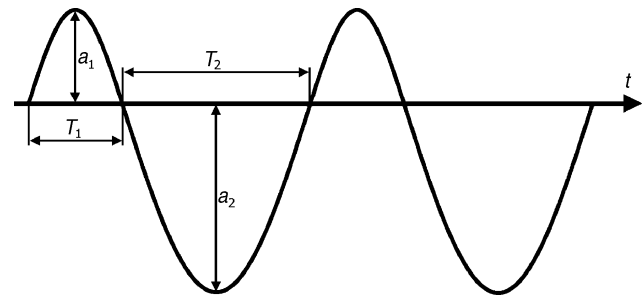

Figure 7. General view of displacement time history in a vibratory system with piecewise rigidity equation (5).
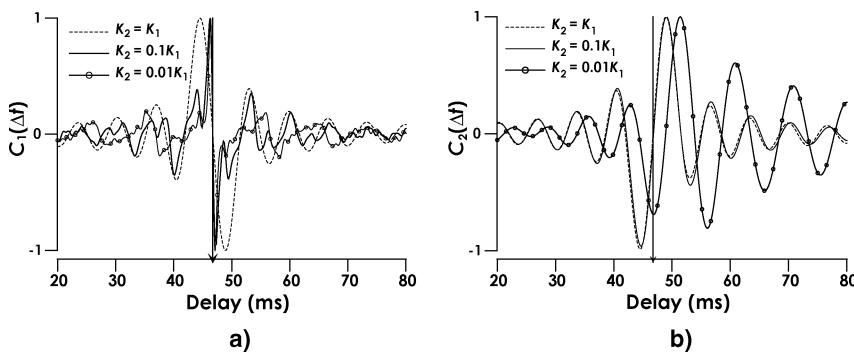

a)

b)

Figure 6. Crosscorrelations between (a) the far-field signal defined by equation (B-6) and the ground-reaction force defined by equation (2) (similar to the HFVS method), and (b) the far-field signal (B-6) and the pilot signal (conventional data processing). The dashed lines correspond to the linear oscillations ($K_2 = K_1$), and the thin solid lines correspond to nonlinear oscillations. The radiated signal is sweep from 15 to 150 Hz. The traveltime is defined as zero crossing between the first two correlation extremes ($\max |C(\Delta t)|$) (Martin and Jack, 1990) and is shown as the vertical lines with arrows ($\Delta t_0 = |OA|/V_P = 47$ ms).

each driving amplitude is associated with different rigidities. This leads to the different values of frequencies Ω_i and the different phase lags in the correlation function at each force level. We hypothesize that the dependence of traveltime on the driving level, observed by Martin and Jack (1990), may be explained by this mechanism. The detailed analysis of such a general model is beyond the scope of this paper.

NONLINEAR RESPONSE OF SOIL BENEATH THE BASEPLATE

At frequencies $\omega < \omega_2$, which correspond to the small wave size of the baseplate, the ground-reaction force mostly depends on the captured rigidity K_g (Safar, 1984). Its value is determined as

$$K_g = \frac{2Er_0}{1 - \nu^2}, \tag{9}$$

where E and ν are the Young's modulus and Poisson's ratio of the ground (Safar, 1984; Johnson, 1985); respectively. Equation (9) describes the rigidity of the elastic cylinder with radius r_0 and length $\pi r_0/2$, deformed along its axis; the value of K_g is thus controlled by the properties of the ground near the baseplate.

Figure 8 exhibits the distribution of the amplitudes of volumetric and shear stress, which control the level of ground deformation, near the baseplate at 100 Hz. The maximum volumetric stress is 0 dB, and the maximum shear stress is -16 dB. This corresponds to a maximum volumetric and shear strain as small as 7×10^{-6} and 2×10^{-6}, respectively. If we hypothesize that the deviation from the linear response in solids is observed at the strain on the order of 10^{-6} and higher (White, 1983; Guyer and Johnson, 1999), we can conclude from Figure 8 that, even at high frequencies, the large nonlinear deformations occur near the baseplate only. Only a small region beneath the plate is then responsible for the distortion of the signal. The captured rigidity K_g, controlled by the material properties in this region, become a nonlinear function.

This reasoning leads us to the conclusion that the model (3) can be generalized to describe not only a strong nonlinear response in the contact area but also the nonlinear elasticity in the soil itself. One can see from Figure 2 that the two springs K_c and K_g are connected in series. The nonlinear properties of K_g are therefore be revealed in the behavior of z_1, z_2, which define

the ground-reaction force (2), in a similar way as the properties of the contact spring K_c are revealed, at frequencies below ω_2. Note that the frequencies used in seismic exploration are typically in this range. It follows that the nonlinear response of the ground beneath the plate can be described by the same model (3) with the properly characterized rigidity of the nonlinear ground spring K_g. The effects on the radiation will be similar to those for the model of contact nonlinearity.

CONCLUSIONS

The harmonic distortion of the signal generated by a vibratory source resulting from contact nonlinearity can be understood using a simple model. The contact-nonlinearity model used has clear physical meaning: it involves the difference in the restoring force between the compression and tension phases that is typical of structurally inhomogeneous media (Guyer and Johnson, 1999). An additional distortion of the particle-velocity signal, recorded by geophones in the far-field, with respect to the ground force, occurs. In this case, the geophone signal is proportional to the time derivative of the ground force; as a result, all harmonics are amplified.

The use of crosscorrelation function between the ground force and the signal from a geophone in the far-field allows one to make a judgment about the origin of the distortion. If the distortion is localized in the contact area, no changes in the traveltime depending on the driving-force level will be observed.

The nonlinearity of the ground in the near-field of the baseplate can be naturally incorporated into the same model.

ACKNOWLEDGMENTS

APPENDIX A

RADIATED POWER

As shown by Lebedev and Sutin (1996), the following expressions for the power radiated in P- and S-waves from a monochromatic vibrator can be obtained [similar expressions

Figure 8. Stress in soil on a vertical section beneath the baseplate. The vertical axis is the depth, and the horizontal axis is the radial distance from the baseplate center. The problem considered is axisymmetric relative to the z-axis. The vertical arrows show the edge of the baseplate. All values are in decibels with respect to the value of $F_g/\pi r_0^2$, which corresponds to the normal stress. The lines depict the levels of -20, -30, -40, and -50 dB. The calculations were made based on the numerical integration of equations (B-1) and (B-2) and Hooke's law. (a) Volumetric stress. (b) Shear stress.
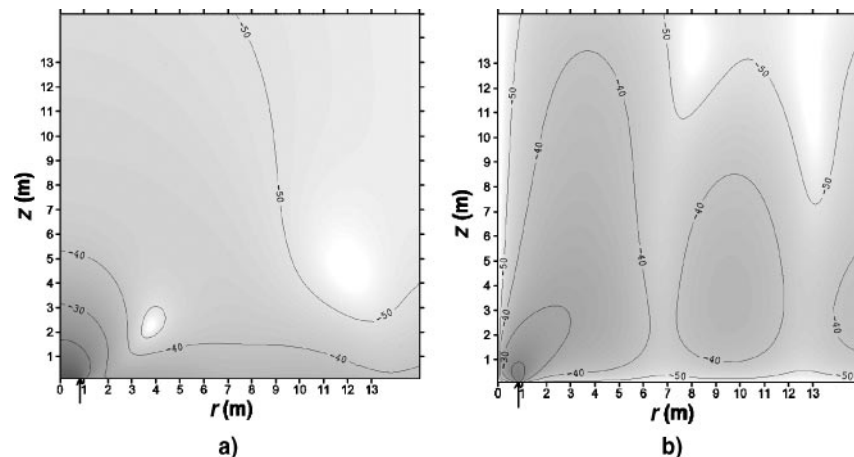
are found in Miller and Pursey (1954)]:

$$W_P = \pi \omega (\lambda + 2\mu) k_1^3 \int_0^{\pi/2} |\phi_P(\theta)|^2 R^2 \sin\theta \, d\theta = \frac{k_1^2 F_g^2}{4\pi\rho c_1} I_1,$$
(A-1)

$$W_S = \pi \omega \mu k_2^3 \int_0^{\pi/2} |\psi_S(\theta)|^2 R^2 \sin\theta \, d\theta = \frac{k_2^2 F_g^2}{4\pi\rho c_2} I_2,$$ (A-2)

where λ and μ are the Lame-constants, $k_j = \omega/c_j$, c_1 is the P-wave velocity, c_2 is the S-wave velocity, ρ is the soil density, and F_g is the amplitude of the ground-reaction force. To calculate the spectral power density of radiated power for non-monochromatic signals, one needs to substitute F_g^2 with the spectral power density of the ground-reaction force for each frequency ω. The functions ϕ_P and ψ_S are the scalar and vector potentials (B-4) and (B-5) (the vector ψ_S is directed clockwise with respect to the z-axis), which are inversely proportional to the distance from the source to the observation point R, and θ is the angle between the radius vector $\mathbf{R}$ and the z-axis (Figure 2). The origin of the coordinate system coincides with the center of the source. The integrals $I_{1,2}$ are

$$I_1 = \int_0^{\pi/2}$$
$$\frac{\Xi_1^2(\theta) \cos^2\theta \sin\theta (1 - 2\gamma^2 \sin^2\theta)^2}{\left(4\gamma^3 \cos\theta \sin^2\theta \sqrt{1 - \gamma^2 \sin^2\theta} + (1 - 2\gamma^2 \sin^2\theta)^2\right)^2} d\theta,$$
(A-3)

$$I_2 = \int_0^{\pi/2} \frac{\Xi_2^2(\theta) \sin^2 2\theta \sin\theta (\gamma^2 - \sin^2\theta)}{\left|2\sin\theta \sin 2\theta \sqrt{\gamma^2 - \sin^2\theta} + \cos^2 2\theta\right|^2} d\theta,$$
(A-4)

with $\gamma = c_2/c_1$ and $\Xi_j(\theta) = 2J_1(k_j r_0 \sin\theta)/(k_j r_0 \sin\theta)$, $j = 1, 2$. The term $J_1(\cdot)$ is the first-order Bessel function, and r_0 is the radius of the baseplate. At low frequencies ($k_j r_0 \ll 1$), the functions $\Xi_{1,2}(\theta)$ are approximately equation to one. The function $\Xi_3(\tau)$ below has the same asymptote.

Similarly, the power radiated in the Rayleigh wave is

$$W_R = \frac{k_2^2 \tau_1^2 F_g^2 \Xi_3^2(\tau_1)}{4\rho c_2 \left(\frac{dD}{d\tau}\Big|_{\tau=\tau_1}\right)^2} \times \left(\frac{(1 - 2\tau_1^2)^2(1 + 4\tau_1^2 - 4\gamma^2)}{\sqrt{\tau_1^2 - \gamma^2}}\right.$$

$$+ \frac{4\tau_1^2(\tau_1^2 - \gamma^2)(4\tau_1^2 - 3)}{\sqrt{\tau_1^2 - 1}} - 4(2\tau_1^2 - 1)$$

$$\times \left.\frac{(1 + 4\tau_1^2 - 2\gamma^2)\sqrt{(\tau_1^2 - \gamma^2)(\tau_1^2 - 1)} + (\tau_1^2 - \gamma^2)(4\tau_1^2 - 1)}{\sqrt{\tau_1^2 - \gamma^2} + \sqrt{\tau_1^2 - 1}}\right)$$
(A-5)

where τ_1 is the real root of the Rayleigh function

$$D(\tau) = (1 - 2\tau^2)^2 - 4\tau^2\sqrt{(\tau^2 - \gamma^2)(\tau^2 - 1)},$$

and where

$$\Xi_3(\tau_1) = \frac{2J_1(k_2 r_0 \tau_1)}{k_2 r_0 \tau_1}.$$

Note that, as follows from equations (A-1), (A-2), and (A-5), the power in the P-, S-, and Rayleigh waves at low frequencies is magnified by a factor proportional to ω^2, relative to the ground-force amplitude, at each radiated frequency. This leads to the magnification in the harmonic content in the far-field signal as discussed in the text in connection with Figure 4.

The terms $\Xi_{2,3}^2$ have the asymptotic behavior of $(k_2 r_0)^{-5}$ for $k_2 r_0 \gg 1$. Therefore, one can expect the decrease in the radiation efficiency in S- and Rayleigh waves at high frequencies. The exception is the P-wave, which dominates the high-frequency radiation. For the P-wave, because the term $\Xi_1^2(\theta) \propto \delta(\theta)/\sin\theta$ for $k_1 r_0 \gg 1$, where $\delta(\theta)$ is Dirac's delta function, the radiation power W_p is equal to

$$W_P = \frac{F_g^2}{2\pi\rho c_1 r_0^2}.$$
(A-6)

Equation (A-6) has no ω-dependent terms. Therefore, no magnification of distortion in the far-field occurs at high frequencies ($k_1 r_0 \gg 1$).

APPENDIX B

WAVEFIELD AT LONG DISTANCES FROM THE SOURCE

The scalar ϕ and the vector ψ potentials of the displacement vector at an arbitrary point of an elastic half-space can be written as the following integrals (Lebedev and Sutin, 1996):

$$\phi = -\frac{F}{2\pi\rho c_2^2}$$
$$\times \int_0^\infty \frac{\Xi(\tau)\tau(2\tau^2 - 1)J_0(x\tau)\exp(iy\sqrt{\gamma^2 - \tau^2})}{D(\tau)} d\tau$$
$$\equiv -\frac{F}{4\pi\rho c_2^2}$$
$$\times \oint_C \frac{\Xi(\tau)\tau(2\tau^2 - 1)H_0^{(1)}(x\tau)\exp(iy\sqrt{\gamma^2 - \tau^2})}{D(\tau)} d\tau,$$
(B-1)

$$\psi = +\frac{iF}{\pi\rho c_2^2}$$
$$\times \int_0^\infty \frac{\Xi(\tau)\tau^2\sqrt{\gamma^2 - \tau^2} J_1(x\tau)\exp(iy\sqrt{1 - \tau^2})}{D(\tau)} d\tau$$
$$\equiv +\frac{iF}{2\pi\rho c_2^2}$$
$$\times \oint_C \frac{\Xi(\tau)\tau^2\sqrt{\gamma^2 - \tau^2} H_1^{(1)}(x\tau)\exp(iy\sqrt{1 - \tau^2})}{D(\tau)} d\tau,$$
(B-2)

where $\Xi(\tau) = 2J_1(k_2 r_0 \tau)/(k_2 r_0 \tau)$; $J_0(\cdot)$ and $J_1(\cdot)$ are the Bessel functions of zero and first orders; $H_0^{(1)}(\cdot)$ and $H_1^{(1)}(\cdot)$ are the Hankel functions of zero and first orders of the first kind; $x = k_2 r$, $y = k_2 z$ are the dimensionless polar coordinates of the observation point; and F is the force applied to the elastic half-space ($F = -F_g$). The contour of integration C is chosen to satisfy the Sommerfeld radiation conditions (Aki and Richards,

1980). Integrals (B-1) and (B-2) contain the contributions of Rayleigh waves [poles of $D(\tau)$] and body waves (stationary points) (Aki and Richards, 1980). The body waves are the most important ones from a seismic exploration standpoint.

Let us consider a limiting case of x, $y \to \infty$, with $x/y = \tan\theta$, $x = k_2 R \sin\theta$, and $y = k_2 R \cos\theta$, where $R = \sqrt{r^2 + z^2}$. For $\chi \gg 1$, the contribution from a stationary-phase point to an integral of the type $\int_C g(t) \exp(\chi f(t)) dt$ is (Aki and Richards, 1980)

$$\int_C g(t) \exp(\chi f(t)) dt = \sum_j \sqrt{\frac{-2\pi}{f''(t_j)\chi}} g(t_j) \exp(\chi f(t_j)),$$
(B-3)

where t_j are the roots of $f'(t) = 0$.

Using expression (B-3) in integrals (B-1) and (B-2), after transformations, one obtains the equations describing the potential of a P-wave (also see Miller and Pursey, 1954),

$$\phi_P = +i \frac{F \Xi_1(\theta) \cos\theta (1 - 2\gamma^2 \sin^2\theta)}{4\gamma^3 \cos\theta \sin^2\theta \sqrt{1 - \gamma^2 \sin^2\theta} + (1 - 2\gamma^2 \sin^2\theta)^2}$$
$$\times \frac{\exp(ik_1 R)}{2\pi\rho\omega c_1 R},$$
(B-4)

and on S-wave

$$\psi_S = +i \frac{F \Xi_2(\theta) \sin 2\theta \sqrt{\gamma^2 - \sin^2\theta}}{2 \sin\theta \sin 2\theta \sqrt{\gamma^2 - \sin^2\theta} + \cos^2 2\theta}$$
$$\times \frac{\exp(ik_2 R)}{2\pi\rho\omega c_2 R}.$$
(B-5)

Equations (B-4) and (B-5) are valid in the far-field only ($k_{1,2}R \gg 1$). The terms $\Xi_{1,2}(\theta)$, defined in Appendix A, describe the directivity patterns resulting from a finite source size. The downgoing P-wave (propagating in the z-direction) produces a vertical particle velocity V_z:

$$V_z \equiv -i\omega \left.\frac{\partial \phi_P}{\partial R}\right|_{\theta=0} = +i \frac{k_1 F \exp(ik_1 R)}{2\pi\rho c_1 R} \times \exp\left(-\frac{k_1 R\eta}{2}\right).$$
(B-6)

We added the term $\exp(-k_1 R\eta/2)$ to equation (B-6) to describe medium dissipation (anelastic attenuation). For harmonic processes, the anelastic losses are usually added as an imaginary part of the corresponding elasticity modulus (Aki and Richards, 1980; White, 1983). Such an approach is valid if the inverse quality factor $\eta \equiv 1/Q$ is much less than unity and the dissipation can be treated as perturbation to the solution without losses. If the force signal F is distorted, this distortion will be magnified in the velocity signal (B-6) as a result of the multiplication by the factor k_1.

APPENDIX C

GREEN'S FUNCTION AND THE RIGOROUS FORMULATION OF PROBLEM (3)

The captured mass, rigidity, and damping factor in the expression for the ground-reaction force

$$-F_g = M_g \ddot{z}_3 + D_g \dot{z}_3 + K_g z_3$$
(C-1)

used in equation (3) are defined for the small wave size of the baseplate (Safar, 1984; Sallas, 1984). This size for higher har-

monics generally is not small. As a result, the values of M_g, K_g, and D_g may not be the same for the harmonics as for the main tone. This is why the approach characterized by equation (C-1) may not be valid for the case when the harmonic distortion is high and the ground reaction resulting from harmonic contribution is compatible with the reaction at the main tone. (The total harmonic distortion parameter D_{NL} for the ground-reaction force is not small.)

To determine the ground-reaction force for the arbitrary wave size of the baseplate, one needs to develop a more general approach, which could be outlined as follows. Integrals (B-1) and (B-2), combined with Hooke's law, allow one to calculate the radiation impedance (Miller and Pursey, 1954, chapter 6) for a monochromatic acting force. The impedance is defined as the ratio of the ground force to the mean value (the baseplate is assumed rigid under vibrations) of the ground velocity over the area of contact πr_0^2. This leads to the following equation for the radiation impedance Z_{inp}:

$$Z_{\text{inp}} \equiv \frac{-F_g}{\dot{z}_3} \equiv \frac{i}{\omega Y(\omega)},$$
(C-2)

where the subscript inp stands for input and where

$$Y(\omega) \equiv \frac{z_3(\omega)}{F_g(\omega)} = \frac{i\omega}{2\pi\rho c_2^3} \int_0^{+\infty} \frac{\tau\sqrt{\gamma^2 - \tau^2}}{D(\tau)} \Xi^2(\tau) d\tau.$$
(C-3)

One can see that $Y(\omega)$, by its definition, is the transfer function for the average displacement $z_3(\omega)$ (the output) obtained from the ground force $F_g(\omega)$ (the input) at each emitted frequency.

First, let us ensure that the field calculations based on equations (C-2) and (C-3) accurately match the known power radiation characteristics of equations (A-1), (A-2), and (A-5). The total radiation power $(W_P + W_S + W_R)$ is equal to (Aki and Richards, 1980)

$$W = Re\left(\frac{|F_g|^2}{2Z_{\text{inp}}}\right).$$
(C-4)

The numerical evaluation of integral (C-3) shows that, at low frequencies, radiation impedance behaves as $Z_{\text{inp}} \cong iK_g/\omega$, with K_g as defined in equation (9). From equation (C-4), the radiated power is then proportional to $F_g^2 \omega^2$ or has the same frequency dependence as equations (A-1), (A-2), and (A-5) at low frequencies. Similarly, at high frequencies $Z_{\text{inp}} \cong \rho c_1 \pi r_0^2$, and equation (C-4) leads to the expression identical to expression (A-6), also derived from equations (A-1), (A-2), and (A-5) as their combined high-frequency limit. This shows that the solution (C-2)–(C-3) indeed ensures the required behavior of radiated power.

One can also see that the difference in the frequency dependence of F_g/F_a between the accurate solution based on expressions (C-2) and (C-3) and the approximation of the ground-reaction force in the form (C-1) (thick and thin lines in Figure 3) is small enough to be neglected even at high frequencies, where the baseplate is no longer small compared to the wavelengths; at low frequencies, the two solutions simply coincide.

Let us now finalize building the general solution. Based on expressions (C-2) and (C-3), the ground force for the arbitrary wave size of the plate and arbitrary displacement can be obtained as follows. Green's function, which, by definition, is the time-domain equivalent of the transfer function, is equal to

the inverse Fourier transform of $Y(\omega)$. To convert the average displacement of the plate into the ground-reaction force [the inverse of expression (C-3)], we use $1/Y(\omega)$. Green's function becomes

$$G(t) = \frac{1}{2\pi} \int_{-\infty}^{+\infty} \frac{\exp(-i\omega t)}{Y(\omega)} d\omega, \qquad \text{(C-5)}$$

where $Y(\omega)$ is defined by expression (C-3).

Finally, the ground-reaction force for arbitrary $z_3(t)$ is Duhamel's integral (the convolution of Green's function and z_3):

$$-F_g(t) = G(t) \otimes z_3(t) \equiv \int_{-\infty}^{t} G(t-\zeta) z_3(\zeta) d\zeta. \quad \text{(C-6)}$$

This determines the ground-reaction force in a general case. The expression for the ground-reaction force (C-1), used in the last equation in system (3), should then be substituted with expression (C-6); as a result, the last equation in system (3) is rewritten as $G(t) \otimes z_3(t) + F_c(t) = 0$. System (3) will become a set of nonlinear integro-differential equations, which is much more difficult to solve than the set of original differential equations (3).

REFERENCES

Aki, K., and Richards, P. E., 1980, Quantitative seismology, theory and methods: W. H. Freeman and Company.
Allen, K. P., 1996, High fidelity vibratory source seismic method: U.S. patent 5 550 786.
Allen, K. P., Johnson, M. L., and May, J. S., 1998, High fidelity vibratory seismic (HFVS) method for acquiring seismic data: 68th Annual International Meeting, SEG, Expanded Abstracts, 140–143.
Beresnev, I. A., and Nikolaev, A. V., 1988, Experimental investigations of nonlinear seismic effects: Physics of the Earth and Planetary Interiors, **50**, 83–87.
Beresnev, I. A., Nikolaev, A. V., Solov'yev, V. S., and Shalashov, G. M., 1986, Nonlinear phenomena in seismic surveying using periodic vibrosignals: Izvestiya Acad. Sci. USSR, Fizika Zemli (Physics of the Solid Earth), **22**, 804–811.
Chichinin, I. S., 1984, Vibratory radiation of seismic waves (in Russian): Nedra Publishers.

Dimitriu, P. P., 1990, Preliminary results of vibrator-aided experiments in non-linear seismology conducted at Uetze, F. R. G.: Physics of the Earth and Planetary Interiors, **63**, 172–180.
Guyer, R. A., and Johnson, P. A., 1999, Nonlinear mesoscopic elasticity: Evidence for a new class of materials: Physics Today, **52**, No. 4, 30–36.
Jeffryes, B. P., 1996, Far-field harmonic measurement for seismic vibrators: 66th Annual International Meeting, SEG, Expanded Abstracts, 60–63.
Johnson, K. L., 1985, Contact mechanics: Cambridge University Press.
Landau, L. D., and Lifshitz, E. M., 1976, Mechanics: Pergamon Press.
Landau, L. D., Lifshitz, E. M., Kosevich, A. M., and Pitaevskii, L. P., 1986, Theory of elasticity: Pergamon Press.
Lebedev, A. V., and Sutin, A. M., 1996, Excitation of seismic waves by an underwater sound projector: Acoustical Physics, **42**, 716–722.
Lerwill, W. E., 1981, The amplitude and phase response of a seismic vibrator: Geophysical Prospecting, **29**, 503–528.
Mahfouz, I. A., and Badrakhan, F., 1990, Chaotic behavior of some piecewise-linear systems: part I—Systems with asymmetric elasticity: Journal of Sound and Vibrations, **143**, 255–288.
Martin, J. E., and Jack, I. G., 1990, The behavior of a seismic vibrator using different phase control methods and drive level: First Break, **8**, 404–414.
Merritt, H. E., 1967, Hydraulic control systems: John Wiley & Sons, Inc.
Miller, G. F., and Pursey, H., 1954, The field and radiation impedance of mechanical radiators on the free surface of a semi-infinite isotropic solid: Proceedings of the Royal Society (London), **A223**, 521–541.
Naugolnykh, K. A., and Ostrovsky, L. A., 1998, Nonlinear wave processes in acoustics: Cambridge University Press.
Ostrovsky, L. A., and Starobinets, I. M., 1995, Transitions and statistical characteristics of vibrations in a bimodular oscillator: Chaos, **5**, 496–500.
Rudenko, O. V., and Vu, C. A., 1994, Nonlinear acoustic properties of a rough surface contact and acoustodiagnostics of a roughness height distribution: Acoustical Physics, **40**, 593–596.
Safar, M. H., 1984, On the determination of the downgoing P-waves radiated by the vertical seismic vibrator: Geophysical Prospecting, **32**, 392–405.
Sallas, J. J., 1984, Seismic vibrator control and the downgoing P-wave: Geophysics, **49**, 732–740.
Sallas, J. J., and Weber, R. M., 1982, Comments on "The amplitude and phase response of a seismic vibrator" by W.E. Lerwill: Geophysical Prospecting, **30**, 935–938.
Shneerson, M. B., and Mayorov, V. V., 1980, Land seismic exploration using unexplosive sources (in Russian): Nedra Publishers.
Solodov, I. Y., 1998, Ultrasonic of non-linear contacts: Propagation, reflection and NDE-applications: Ultrasonics, **36**, 383–390.
Walker, D., 1995, Harmonic resonance structure and chaotic dynamics in the earth-vibrator system: Geophysical Prospecting, **43**, 487–507.
White, J. E., 1983, Underground sound, application of seismic waves: Elsevier Science Publishing Company, Inc.